IEEE Access
Multidisciplinary | Rapid Review | Open Access Journal

Received April 30, 2020, accepted May 19, 2020, date of publication May 26, 2020, date of current version June 8, 2020.

Digital Object Identifier 10.1109/ACCESS.2020.2997872

Study on the Sensitization Effect of Flywheel-Like Diaphragm on Fiber-Optic Fabry-Perot Acoustic Sensor

XIAOGUANG QI, SHUANG WANG, JUNFENG JIANG, KUN LIU, PENG ZHANG, ZHIYUAN LI, AND TIEGEN LIU

School of Precision Instrument and Opto-electronics Engineering, Tianjin University, Tianjin 300072, China
Key Laboratory of Opto-electronics Information Technology, Ministry of Education, Tianjin 300072, China
Tianjin Optical Fiber Sensing Engineering Center, Institute of Optical Fiber Sensing, Tianjin University, Tianjin 300072, China

Corresponding authors: Shuang Wang (shuangwang@tju.edu.cn) and Junfeng Jiang (jiangjfjxu@tju.edu.cn)

This work was supported in part by the National Natural Science Foundation of China under Grant 61735011, Grant 61675152, and Grant 61505139, and in part by the National Instrumentation Program of China under Grant 2013YQ030915.

ABSTRACT A flywheel-like sensitive diaphragm, which breaks the sensitivity limitations imposed by the increased thickness and the decreased radius in edge-clamped circular structure, has been proposed and analyzed in fiber Fabry-Perot (FP) acoustic sensor. A new model is built around the effect of diaphragm's structure parameters on sensitivity of a fiber FP acoustic sensor with common ductile material. The proposed sensor based on flywheel-like stainless diaphragm in 5mm diameter and 0.035mm thickness has been fabricated and its acoustic performances were tested. The test results show that our acoustic sensor can realize acoustic measurement from 0.1 kHz to 19 kHz. The sensor exhibits an acoustic pressure sensitivity of 1.525nm/Pa at the frequency of 4.5 kHz. The noise-limited minimum detectable pressure (MDP) level of $\sim 13.06 \mu Pa/\sqrt{Hz}$@4.5kHz and the acoustic pressure signal-to-noise ratio (SNR) of 70.42dB@4.5kHz are achieved, respectively. And the mean SNR of cavity length variation of 62.43dB can be acquired over the entire frequency range. Comparing with the edge-clamped circular structure, the flywheel-like structure endows the common ductile sheet material the ability to response to acoustic pressure. Cost-effective and compact size give the proposed acoustic sensor a competitive edge, something of crucial importance to commercial applications.

INDEX TERMS Acoustic sensors, Fabry-Perot, flywheel-like diaphragm.

I. INTRODUCTION

Fiber optic acoustic sensor has shown its great potential in recent decades [1]–[12] because of their unique advantages such as immunity to electromagnetic interference, high resolution, fast response, and compact size. Fiber-tip Fabry-Perot (FP) interferometers (FPI) between a cleaved fiber end and a sensitive diaphragm have demonstrated high sensitivity without the need for a long length of optical fiber compared with Mach-Zehnder interferometers [1] and Michelson interferometers [2]. The sensitivity of the diaphragm in the FP acoustic sensor is defined as the ratio of the length variation of the FP cavity to the acoustic pressure. So various kinds of diaphragm materials have been studied for FPI acoustic sensors, such as silicon [3], silica [4], chitosan [5], silk fibroin [6], UV adhesive [7], silver [8], graphene [9], aluminum [10] and Parylene-C [11]. The abovementioned sensing diaphragms are usually edge-clamped circular structure. The sensor's acoustic pressure sensitivity is proportional to a^4/h^3, where a is the radius and h is the thickness of the diaphragm [8]. Therefore, the diaphragms are typically oriented toward larger radius and smaller thickness to improve the sensor's sensitivity. Gong *et al.* demonstrated an acoustic sensor based on a Parylene-C diaphragm of 9 mm in diameter and 2.4 nm in thickness, with a sensitivity of 2239 nm/Pa at the frequency of 20 Hz [11]. Ni *et al.* demonstrated a FPI acoustic sensor based on an ultrathin graphene diaphragm with a thickness of 10nm, and the noise-limited minimum detectable pressure (MDP) level of $0.77\text{Pa}/\sqrt{\text{Hz}}$@5Hz and $33.97 \mu Pa/\sqrt{\text{Hz}}$@10kHz can be achieved [9]. However, the larger radius and smaller thickness of diaphragm increases the cost and difficulty of the manufacture process, and reduces the sensor's mechanical strength.

The associate editor coordinating the review of this manuscript and approving it for publication was Sukhdev Roy.

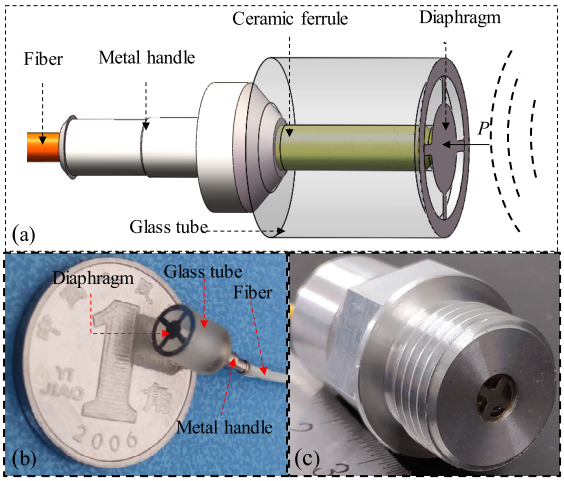

FIGURE 1. The sensor's structure and package, (a) Schematic diagram of sensing head structure, (b) The image of sensing head, (c) The image of sensor's package.

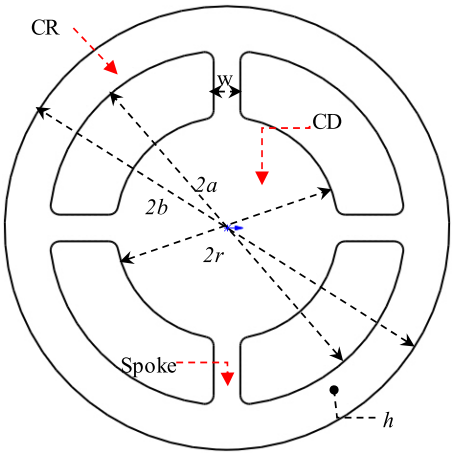

FIGURE 2. The schematic diagram of the flywheel-like diaphragm.

Recently, the researchers have proposed and demonstrated a novel diaphragm structure based on cantilever used in FPI acoustic sensor. Liu *et al.* proposed a FPI acoustic sensor based on a silica micro-cantilever beam fabricated by femtosecond (fs) laser micromachining, and the acoustic pressure sensitivity of 9.75μm/MPa is achieved at the resonant frequency of 0.74 MHz [3]. Chen *et al.* proposed a stainless cantilever beam based FPI acoustic sensor and achieved a pressure responsivity of 211.2 nm/Pa at the frequency of 1 kHz [12]. However, cantilever based diaphragm structure has bred new challenges, that is operation only in the frequency region below the resonance frequency [13] and nonlinear response [14].

In this paper, a cost-effective stainless flywheel-like diaphragm is proposed and its sensitization effect induced by structure parameter is discussed. The FPI acoustic sensor with flywheel-like diaphragm has shown three merits: (1) the flywheel structure breaks the sensitivity limitations imposed by the increased thickness and the decreased radius in edge-clamped circular structure, (2) the flywheel-like structure endows the common ductile sheet material (such as stainless, copper, and aluminum) the ability to response to acoustic pressure, (3) cost-effective (in materials and crafts) and compact size give the FPI acoustic sensor a competitive advantage in commercial applications. The experimental results indicate that the proposed sensor has a sensitivity of 1.525nm/Pa @ 4.5 kHz and a noise-limited MDP of $\sim 3.06\mu Pa/\sqrt{Hz}$@4.5kHz. A mean SNR of 62.43dB can be achieved in the frequency response range of 0.1 kHz ~19 kHz. The proposed flywheel-like sensitive diaphragm is believed to have a bright application prospect.

II. THEORETICAL ANALYSIS OF ACOUSTIC SENSOR

Fig. 1(a) is the schematic of our acoustic sensing head that comprises of a fiber, a metal handle, a ceramic ferrule, a glass tube, and a flywheel-like diaphragm. First, the flywheel-like diaphragm was fixed on one end of a glass tube using epoxy adhesive. Then, a fiber cladded with metal handle and ceramic ferrule have been inserted from the another end of the glass tube, as shown in the Fig.1 (b). Finally, the sensing head is enclosed in an aluminum housing, as shown in the Fig.1 (c). Throughout the process, the epoxy adhesive plays a role in pre-fixation, and all the components are connected and fastened, via a screw-thread on the metal shell. As the Fig.1 shows, there are many hollowed-outs on the diaphragm that endow to keep the balance of internal and external pressure. The flywheel-like diaphragm was produced in bulk using the laser engraving technology. Hence, the flywheel-like structure apply to all common ductile sheet material such as stainless, copper, and aluminum. Compared with ultra-thin novel materials and circular structure [3]–[11], inexpensive materials and simple crafts give a competitive advantage to the proposed sensor in commercial applications. In addition, the proposed sensing head only has a boundary size of 5mm × 11mm (diameter × length), which makes is more convenient in encapsulation for meeting various application scenarios.

A. DYNAMIC PROPERTIES OF FLYWHEEL-LIKE DIAPHRAGM

As a dynamic signal, the acoustic wave needs to be transformed into detectable physical parameter by the sensitive diaphragm. Thus the diaphragm is a critical component to the acoustic sensor based on FPI structure. The diaphragm will have a deformation when the acoustic waves are loaded. Therefore, the acoustic waves is finally converted to the synchronous variation of cavity length of FPI and the two frequencies are consistency. As illustrated in Fig. 2, the diaphragm was carved into flywheel shape in stainless sheet. The flywheel-like diaphragm consists of three components: circle ring (CR), spoke, and central diaphragm (CD). The diaphragm was fixed on the glass tube via the CR. So the vibration model of flywheel-like diaphragm can be analyzed according to the leaf-spring hinge [15]. According to the dynamic principles, the deflection $l(t)$ of a flywheel-like

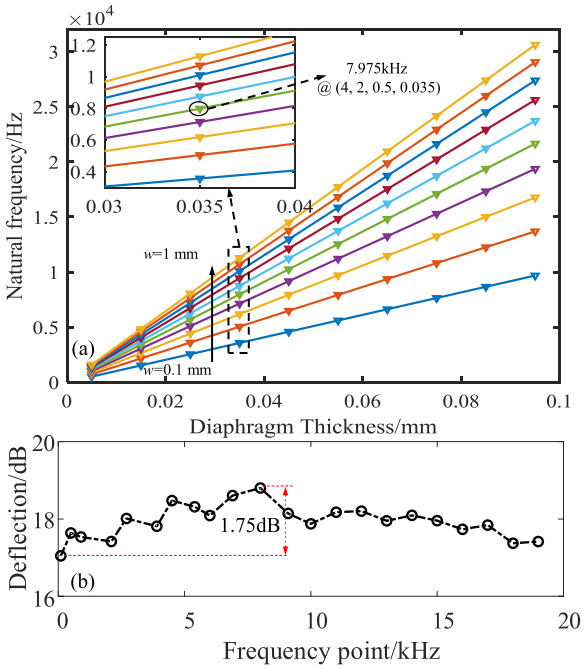

FIGURE 3. The simulation results of flywheel-like stainless diaphragm: (a) natural frequency calculated by Eq. (3), (b) frequency response curve simulated by ANSYS.

diaphragm must meet with the motion equation, that is

$$m\ddot{l}(t) + \beta\dot{l}(t) + kl(t) = \pi r^2 P(t) \tag{1}$$

where $m = \rho\pi r^2 h$ is weight of proof mass, ρ, h and r are the material density, diaphragm's thickness and CD's radius, respectively. β is the damping coefficient of acoustic wave in air, k is spring constant of the flywheel-like diaphragm, $P(t)$ (in Pa) is the acoustic pressure acting on the diaphragm, t is a time parameter.

The pressure response of flywheel-like diaphragm, which is the solution of Eq. (1), can be expressed as

$$l(\omega, t) = \frac{\pi r^2 P(t)}{m\sqrt{\left(\omega_0^2 - \omega^2\right)^2 + (\omega\beta/m)^2}} \tag{2}$$

where $l(\omega, t)$ is the maximum deformation of the flywheel-like diaphragm at the angular frequency ω, $P(t)$ is the time domain acoustic pressure under the frequency $\omega/2\pi$. ω_0 is the natural angular frequency, which can be calculated by the Eq. (3) and Eq. (4) [15].

$$\omega_0 = \sqrt{\frac{k}{m}} \tag{3}$$

$$k = \frac{4Ewh^3}{(a-r)^3} \tag{4}$$

where in Eqs. (3) and (4) k is spring constant, E is the Young's modulus of the diaphragm, w and $2a$ are the spoke's width and the CR's inner diameter, respectively.

Based on the Eq. (3) and (4), the varying curves of natural frequency of flywheel-like stainless diaphragm with its structural parameters can be calculated. Fig.3 (a) has described

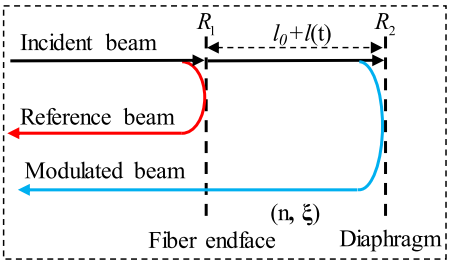

FIGURE 4. The propagation model of the proposed acoustic sensor based on FPI.

the numerical simulation results of the natural frequency variation with the diaphragm's thickness (h) and spoke's width (w). As we can see that our sensor's theoretical natural frequency can be tailored by changing the diaphragm's structure parameters. In our sensor configuration, a flywheel diaphragm fabricated by a structure parameters combination [4, 2, 0.5, 0.035] (in mm) (corresponding to CR's inner diameter $2a$, CD's diameter $2r$, spoke's width w, and diaphragm's thickness h) has been used to assemble the fiber FP acoustic sensor. In this case, a theoretical natural frequency of the proposed sensor is 7.975 kHz. And the diaphragm's theoretical response curve simulated by ANSYS soft is shown in the Fig.3 (b). And we can see that the diaphragm has a flat frequency responsivity and the fluctuating range is 1.75dB.

The acoustic pressure response sensitivity $S_a(\omega, t)$ of the proposed sensor is defined as the ratio of the deflection $l(\omega, t)$ of a flywheel-like diaphragm to the acoustic pressure $P(t)$ at the frequency of ω, which is written as:

$$S_a(\omega, t) = \frac{l(\omega, t)}{P(t)} \tag{5}$$

The Eqs. (2) $\sim$ (5) reveal that the acoustic pressure response sensitivity $S_a(\omega, t)$ of the proposed sensor is closely related to the structure parameters of a flywheel-like diaphragm.

B. OPTICAL PRINCIPLES OF ACOUSTIC SENSOR

As illustrated in Fig. 4, the proposed acoustic sensor is comprised of two mirrors. The first one is the fiber end-face and the second one is flywheel-like diaphragm. The incident beam was divided two beams at the fiber end-face. The first beam reflected by fiber end-face is referred to as reference beam. Another beam propagates along the FP cavity and reflected back by the diaphragm as modulated beam. The returning light beams merge together at fiber end-face and create an interference signal. Due to the smaller reflectivity of R_1 and R_2 of the fiber end-face and the flywheel-like diaphragm, the propagation model of the proposed acoustic sensor can be analyzed according to the two-beam interference. So the interference intensity I_r in the FP cavity can be approximated as [16]:

$$I_r = (R_1 + \xi R_2 - 2\sqrt{\xi R_1 R_2}\cos\varphi) I_i \tag{6}$$

where ξ is the loss coefficient of FP cavity; $\varphi = 4\pi n l_0/\lambda$ is the phase difference, where n, l_0, and λ are the refractive index, the initial cavity length, and the operating wavelength,

respectively; I_i is the intensity of incident beam. According to the analysis of FP cavity length loss [17], ξ can be determined by:

$$\xi = \frac{4[1 + (\frac{2\lambda l_0}{\pi n \omega_0^2})^2]}{[2 + (\frac{2\lambda l_0}{\pi n \omega_0^2})^2]^2} \tag{7}$$

where ω_0 is the mode field radius. For a single-mode fiber and an air medium, ω_0 and n are set as 4.9μm and 1, respectively. Thus, ξ is a function of λ and l_0.

During the interference intensity demodulation, the variation of light intensity ΔI caused by the cavity length fluctuation Δl can be expressed as follows:

$$\Delta I = I_r - I_r' = \frac{8\pi n}{\lambda} I_i \sin \frac{4\pi n l_0}{\lambda} \sqrt{\xi R_1 R_2} \Delta l \tag{8}$$

where I_r is the interference intensity modulated by acoustic pressure, I_r' is the interference intensity in absence of acoustic pressure. According to the Eq. (8), we can see that the variation of light intensity received by the photo-detector (PD) is proportional to the cavity length fluctuation caused by acoustic pressure. A similar conclusion has been reached in Ref. [16], [19]. Because our acoustic sensor's initial cavity length is available to be tuned to the operating point of an interference fringe to maximize the optical sensitivity during the interference intensity demodulation, the phase difference $\varphi = 4\pi n l_0 / \lambda$ may be adjusted to be $(k + 1/2)\pi$, where k is a nature number. In the intensity demodulation system, the interference intensity I_r is finally converted to the output voltage of the PD. Assuming that the output voltage V_r from the PD is defined as:

$$V_r = \eta I_r \tag{9}$$

where η is the responsivity of the InGaAs photo-detector, ~1.07 A/W at 1550 nm [20]. Then, in combination with Eqs (8) and (9), the cavity length fluctuation Δl caused by acoustic pressure is derived as

$$\Delta l = \frac{\lambda(R_1 + \xi R_2)}{8\pi n V_0 \sqrt{\xi R_1 R_2}} (V_r - V_0) \tag{10}$$

where V_0 is the output voltage from the PD in absence of acoustic pressure. Thus, the pressure deflection behavior of the proposed acoustic sensor can be measured to analyze its acoustic pressure sensitivity.

In our sensor configuration, the interference spectrum measured by a broadband source in combination with the AQ6370C having a wavelength resolution of 0.02nm, as shown in Fig. 5. According to the interference spectrum, a double-peak phase demodulation method was performed to set the initial cavity length as 85.3768μm. Moreover, the reflectivity R_1 of the fiber end-face was calculated as 3.37% by using the Fresnel reflection and the effective reflectivity R_2 of the stainless diaphragm was calculated as 0.5992% from the visibility of interference fringes in Fig. 5. Then, ξ in the Eq. (8) and Eq. (10) was calculated as 0.2 by using the Eq. (7).

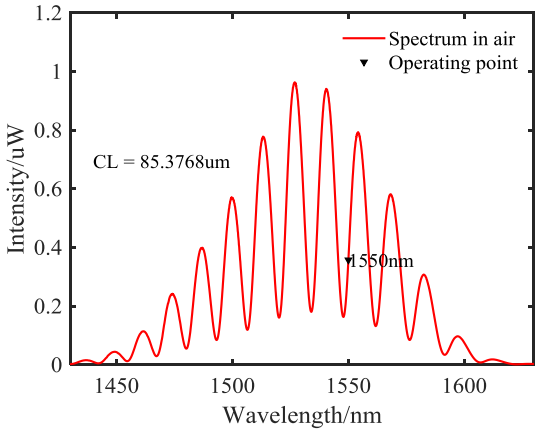

FIGURE 5. Interference spectra of the proposed acoustic sensor in air.

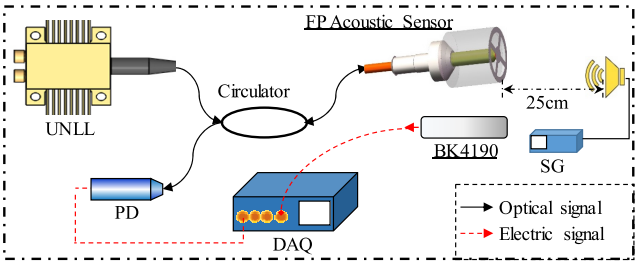

FIGURE 6. Experimental setup to test the proposed sensor response to acoustic wave.

III. EXPERIMENT AND ANALYSIS

According to the analysis of section II, an experimental setup based on an intensity demodulation method has been built to test the proposed sensor response to acoustic wave, as shown in Fig. 6. The experimental apparatus mainly includes 1550nm ultra-narrow linewidth laser (UNLL, power stability $\leq \pm 0.05$dB in 8hour, wavelength stability $\leq \pm 1$pm) [18], circulator, acoustic sensor, InGaAs photo-detector (PD), loud-speaker, signal generator (SG), reference acoustic sensor (Type 4190, Brüel & Kjær) [21], data acquisition (DAQ) card. The laser beam emitting from UNLL is launched into a circulator, and then propagates into the acoustic sensor. The acoustic wave emitted by the loud-speaker deforms the diaphragm, leading to changes of the FP cavity length. A PD is used to detect the interferometric signal. Then the cavity length variation can be demodulated from the changes of the output signal intensity by the interferometric intensity demodulation mechanism based on the Eq. (10). Furthermore, the acoustic field evoked by the loud-speaker can be modulated by the SG. And the acoustic field characteristics (such as frequency and intensity) can be calibrated by the reference sensor. In order to ensure synchronous measurement, our acoustic sensor and the reference sensor are located side by side and they are placed opposite to the loud-speaker, and the distance is about 25cm. When no acoustic pressure is imposed on the diaphragm, the output voltage from the PD is defined as the system noise levels V_0 and the mean values of the repeated measures is 0.016mV.

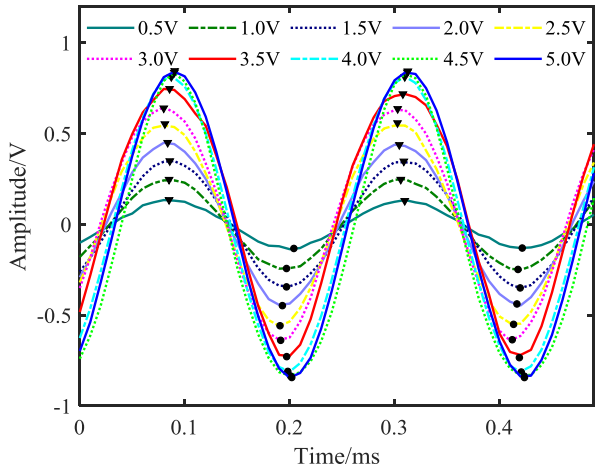

FIGURE 7. Output signal of the acoustic sensor vary with different amplitudes of the excitation signal at the frequency of 4.5 kHz.

A. ACOUSTIC PRESSURE RESPONSE

To test the sensor's acoustic pressure response, the amplitude of a sinusoidal excitation signal sent by the SG with the frequency of 4.5 kHz changes from 0.5V to 5.0V. So we achieved a varying acoustic field modulated by the excitation signal. In this case, the output signal of the acoustic sensor changes with different amplitudes of the excitation signal as shown in Fig. 7. And a similar tendency of output signal has been found in the reference sensor (BK4190). The output signal amplitude of our acoustic sensor and BK4190 were respectively depicted by the blue dotted curve and red solid curve in Fig. 8(a).

Obviously, our sensor and BK4190 have a similar output response to the modulated acoustic field. The reason for nonlinear region is that loud-speaker's output is no longer linear in 4V $\sim$ 5V. And the red solid curve in the Fig.8 (b) has described the acoustic pressure changes in different excitation signal's voltage. Based on the Eq. (10), the variation of FP cavity length can be calculated as the blue dotted curve in Fig.8 (b). We can clearly see that the variation of FP cavity length was consistent with the acoustic pressure. Hence, the pressure sensitivity of our acoustic sensor can be calculated as 1.525nm/Pa by the slope ratio of two fitting curves in Fig.8 (b). For an edge-clamped circular stainless diaphragm, the pressure sensitivity can be calculated by the formula of $S = 3(1-\sigma^2)(2a)^4/256Eh^3$ [19], where $2a = 5mm$ and $h = 0.035mm$ are respectively the diameter and the thickness, and $\sigma = 0.247$ and $E = 201GPa$ are respectively the Poisson ratio and Young's modulus of the stainless diaphragm. The theoretical pressure sensitivity in terms of acoustic pressure-induced deflection is calculated to be $2.79 \times 10^{-3} nm/Pa$. So there is good reason to believe that the flywheel-like structure endows diaphragm with excellent acoustic pressure response performance under the same conditions (such as material and structure parameter). Moreover, Fig. 8(a) has also indicated that the output signal's pressure sensitivity is 1.39 times higher than that revealed by the reference sensor (BK4190) in the same acoustic field.

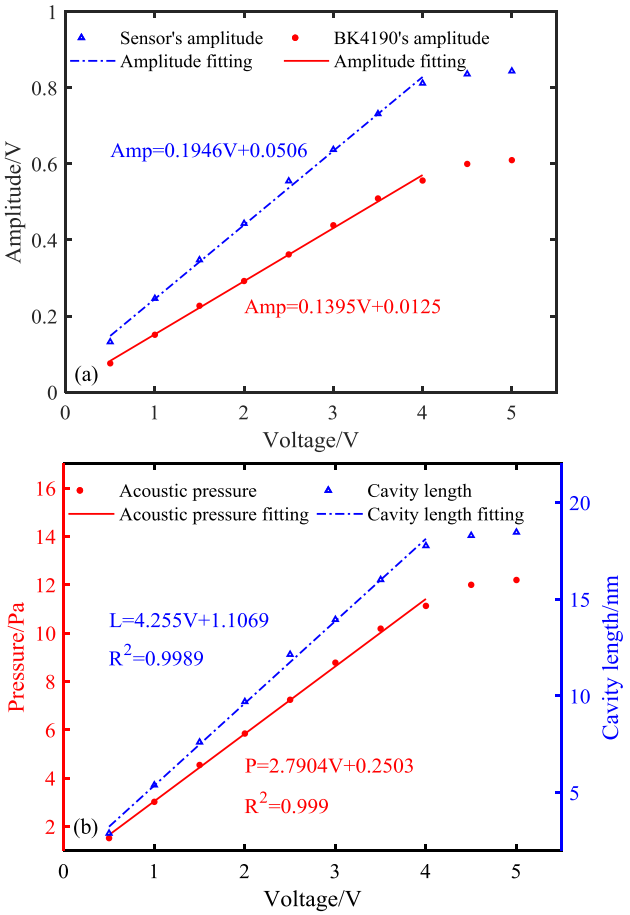

FIGURE 8. Under the different excitation signal voltage, (a) the output signal's amplitude comparison of our acoustic sensor and BK4190, (b) our sensor's measured cavity length variation (the blue dotted curve) and the calibration acoustic pressure by BK4190 (the red solid curve).

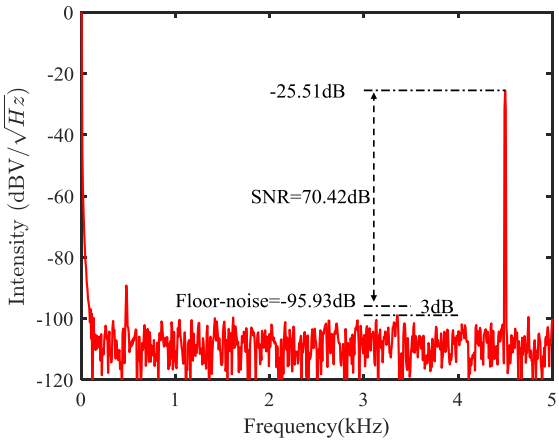

FIGURE 9. Frequency response of our sensor's output signal at 4.5 kHz.

Fig. 9 shows power spectral density (PSD) of our sensor's output signal when a sinusoidal excitation signal's amplitude of 3V at 4.5 kHz is applied. We can see that our sensor's floor-noise is as low as −95.93dB and the signal to noise ratio (SNR) is 70.42dB at the frequency of 4.5 kHz. According to previous research results [22], [23],

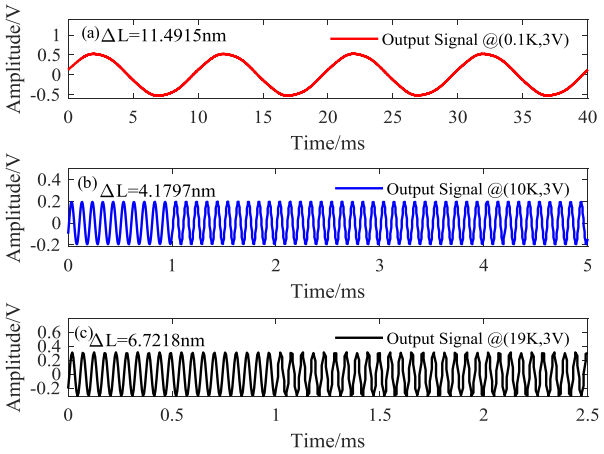

FIGURE 10. The sensor's output singal detected by the PD are respectively (a) 0.1 kHz, (b) 10 kHz, and (c) 19 kHz.

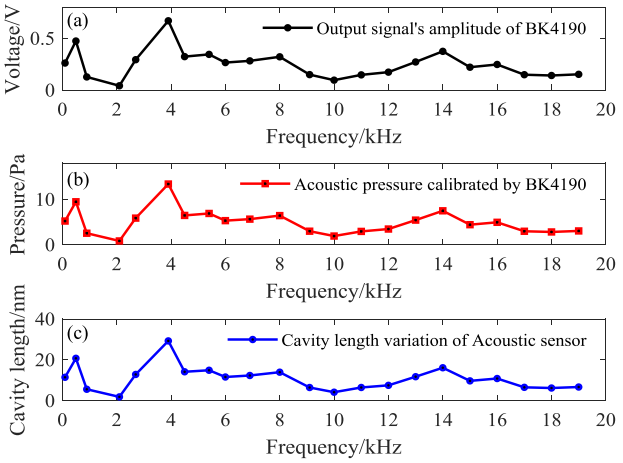

FIGURE 11. The output responses under different frequencies and the acoustic pressure curve. (a) The output response of BK4190. (b) The acoustic pressure curve calibrated by BK4190. (c) The output response of our acoustic sensor.

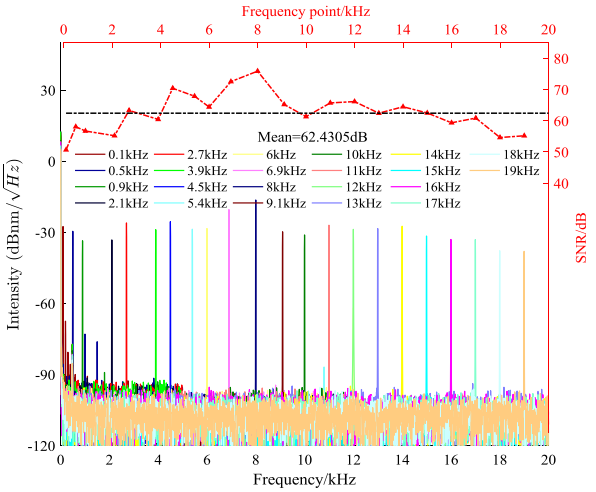

FIGURE 12. Power density spectrum of the cavity length variation in different frequencies and their corresponding SNR.

the noise-limited minimum detectable pressure (MDP) of the sensor (in $Pa/\sqrt{Hz}$) is by definition the incident acoustic pressure that induces an output signal equal to the noise. It is equal to the noise spectral density of the sensor (in $V/\sqrt{Hz}$) divided by the calibrated sensor response sensitivity (in V/Pa). In our experimental configuration, the sensor's output voltage in absence of acoustic pressure is recorded and calculated its noise spectral density. Then our sensor's MDP is $\sim 13.06 \mu Pa/\sqrt{Hz}$ at $4.5kHz$.

B. ACOUSTIC FREQUENCY RESPONSE

To test the sensor's acoustic frequency response, a broadband frequency sweep experiment has been performed. In this case, the frequency of a sinusoidal excitation signal sent by the SG with the amplitude of 3V changes from 0.1 kHz to 19 kHz. The PD is used to record the sensor's output signal at different frequencies. And then the variation of sensor's cavity length calculated by the Eq. (10) is regarded as the frequency response. Fig.10 has depicted the sensor's output signal, when the frequency of an excitation signal with the amplitude of 3V are 0.1 kHz, 10 kHz and 19 kHz, respectively.

Over the entire test frequency range, our sensor has a good acoustic fidelity, as indicated by the output waveform showing good agreement with excitation signal. In these conditions, our sensor's cavity length variation can be achieved 11.4915nm, 4.1797nm and 6.7218nm, respectively.

Moreover, Fig. 11(a) shows the output signal's amplitude of the reference sensor (BK4190). Based on that curve, we can calibrate the acoustic pressure curve [see Fig. 11(b)] generated by loud-speaker under the excitation signal's frequency changes from 0.1 kHz to 19 kHz at amplitude of 3V. Our sensor's cavity length variation in the action of acoustic pressure shows in the Fig. 11(c). By comparing the response curves of reference sensor (BK4190) and acoustic sensor in Fig. 11, we can see that our sensor's cavity length variation is consistent with acoustic pressure changes measured by reference sensor. Therefore, we consider that our acoustic sensor and reference sensor (BK4190) have a similar frequency response in the range of 0.1 $\sim$ 19 kHz.

To further test the sensor's characteristic in frequency domain, the power density spectrum of the cavity length variation is carried out, as the color-curves shown in Fig 12. The red dotted line indicates the SNR of sensor's cavity length variation in frequency domain. And we can see that the peak of sensor's cavity length variation occurs at $\sim$8 kHz, which is very near the natural frequency of 7.975 kHz. Moreover, the mean SNR of cavity length variation of 62.4305dB can be achieved in the frequency range of 0.1 kHz $\sim$ 19 kHz.

As shown in Table 1, our acoustic sensor have demonstrated a low MDP ($\sim 13.06 \mu Pa/\sqrt{Hz}$) at 4.5 kHz, a high average SNR (62.43dB) over a fairly broad response range (0.1 kHz to 19 kHz). All these are due to the flywheel-like structure can improve diaphragm's responsiveness to acoustic pressure in fiber FP acoustic sensor. Moreover, low-price diaphragm material (stainless) and simple craft (laser engraving) make the proposed acoustic sensor more attractive in commercial applications.

TABLE 1. Performance of selected acoustic sensors.

Authors (Year)	Response range	Minimum MDP ($\mu Pa/\sqrt{Hz}$)	SNR (dB)	Sensing scheme /Medium	Material / Craft	Ref
*	0.1 kHz~ 19 kHz	~13.06@4.5 kHz	62.43[b]	Fabry-Perot/Air	Stainless/ Laser engraving	*
Brüel & Kjær (2009)	6.3 Hz~ 20 kHz	N/A	N/A	Capacitive/Air	N/A	[21]
Liu et al. (2017)	0.5 MHz~ 4 MHz	N/A	23[a]	Fabry-Perot/Air or water	Silica / Femtosecond laser	[3]
Gao et al. (2019)	0.8 MHz~ 5 MHz	N/A	50[a]	Fabry-Perot/Air	Silica / Femtosecond laser	[4]
Ni et al. (2018)	5 Hz ~ 0.8 MHz	~33.97@10 kHz	<35[b]	Fabry-Perot/Air or water	Graphene/ Chemical vapor deposition	[9]
Fu et al. (2018)	50 Hz ~ 300 Hz	N/A	<40[b]	Fabry-Perot/Air	Aluminum foil/ N/A	[10]
Gong et al. (2017)	7 Hz ~ 1.8kHz	22.1@ 20Hz	N/A	Fabry-Perot/Air	Parylene-C/ Vacuum deposition	[11]

MDP = minimum detectable pressure, SNR = Signal-to-noise ratio, N/A = data not available,
* This article, [a] At a resonance, [b] Averages.

IV. CONCLUSION

In summary, we proposed a novel flywheel-like structure diaphragm used in fiber FPI acoustic sensor. The flywheel-like structure breaks the sensitivity limitations imposed by the increased thickness and the decreased radius of a circular diaphragm used in traditional fiber FPI acoustic sensors. The sensor exhibits an acoustic pressure sensitivity of 1.525nm/Pa at the frequency of 4.5 kHz. The noise-limited MDP of $\sim 13.06\mu Pa/\sqrt{Hz}$@4.5kHz and the acoustic pressure SNR of 70.42dB@4.5kHz are achieved, respectively. And the mean SNR of cavity length variation of 62.43dB can be acquired in the frequency range of 0.1 kHz ~ 19 kHz. Other merits of the proposed sensor are its compact size (diameter × length: 5mm × 11mm) and cost-effective (in materials and crafts). The flywheel-like diaphragm based fiber FP acoustic sensor is believed to have a bright application prospect.

REFERENCES

[1] T. K. Lim, Y. Zhou, Y. Lin, Y. M. Yip, and Y. L. Lam, "Fiber optic acoustic hydrophone with double Mach–Zehnder interferometers for optical path length compensation," *Opt. Commun.*, vol. 159, nos. 4–6, pp. 301–308, Jan. 1999.

[2] K. Atherton, F. Dong, G. Pierce, and B. Culshaw, "Mach–Zehnder optical fiber interferometers for the detection of ultrasound," *Proc. SPIE*, vol. 3986, pp. 27–34, Jun. 2000.

[3] J. Liu, L. Yuan, J. Lei, W. Zhu, B. Cheng, Q. Zhang, Y. Song, C. Chen, and H. Xiao, "Micro-cantilever-based fiber optic hydrophone fabricated by a femtosecond laser," *Opt. Lett.*, vol. 42, no. 13, p. 2459, Jul. 2017.

[4] R. Gao, D.-F. Lu, J. Cheng, and Z.-M. Qi, "Ultrasonic detection of high-intensity focused ultrasound field using quadrature point phase step in a fiber optic interferometric sensor," *J. Lightw. Technol.*, vol. 37, no. 11, pp. 2694–2699, Jun. 1, 2019.

[5] L. H. Chen, C. C. Chan, W. Yuan, S. K. Goh, and J. Sun, "High performance chitosan diaphragm-based fiber-optic acoustic sensor," *Sens. Actuators A, Phys.*, vol. 163, no. 1, pp. 42–47, Sep. 2010.

[6] F. Guo, T. Fink, M. Han, L. Koester, J. Turner, and J. Huang, "High-sensitivity, high-frequency extrinsic Fabry–Perot interferometric fiber-tip sensor based on a thin silver diaphragm," *Opt. Lett.*, vol. 37, no. 9, pp. 1505–1507, May 2012.

[7] L. Liu, P. Lu, S. Wang, X. Fu, Y. Sun, D. Liu, J. Zhang, H. Xu, and Q. Yao, "UV adhesive diaphragm-based FPI sensor for very-low-frequency acoustic sensing," *IEEE Photon. J.*, vol. 8, no. 1, Feb. 2016, Art. no. 6800709.

[8] F. Xu, J. H. Shi, K. Gong, H. F. Li, R. Q. Hui, and B. L. Yu, "Fiber-optic acoustic pressure sensor based on large-area nanolayer silver diaghragm," *Opt. Lett.*, vol. 39, no. 10, pp. 2838–2840, May 2014.

[9] W. J. Ni, P. Lu, X. Fu, W. Zhang, P. P. Shum, H. D. Sun, C. Y. Yang, D. M. Liu, and J. Shan, "Ultrathin graphene diaphragm-based extrinsic Fabry–Pérot interferometer for ultra-wideband fiber optic acoustic sensing," *Opt. Express*, vol. 26, no. 16, pp. 20758–20767, Aug. 2018.

[10] X. Fu, P. Lu, L. Zhang, W. J. Ni, D. M. Liu, and J. S. Zhang, "Analysis on Fourier characteristics of wavelength-scanned optical spectrum of low finesse Fabry–Pérot acoustic sensor," *Opt. Express*, vol. 26, no. 17, pp. 22064–22074, Aug. 2018.

[11] Z. Gong, K. Chen, X. Zhou, Y. Yang, Z. Zhao, H. Zou, and Q. Yu, "High-sensitivity Fabry–Pérot interferometric acoustic sensor for low-frequency acoustic pressure detections," *J. Lightw. Technol.*, vol. 35, no. 24, pp. 5276–5279, Dec. 15, 2017.

[12] K. Chen, Z. H. Yu, Q. X. Yu, M. Duo, Z. H. Zhao, C. Qu, Z. F. Gong, and Y. Yang, "Fast demodulated white-light interferometry-based fiber-optic Fabry–Pérot cantilever microphone," *Opt. Lett.*, vol. 43, no. 14, pp. 3417–3420, Jul. 2018.

[13] V. Koskinen, J. Fonsen, K. Roth, and J. Kauppinen, "Progress in cantilever enhanced photoacoustic spectroscopy," *Vibrational Spectrosc.*, vol. 48, no. 1, pp. 16–21, Sep. 2008.

[14] J. E. Sader, "Frequency response of cantilever beams immersed in viscous fluids with applications to the atomic force microscope," *J. Appl. Phys.*, vol. 84, no. 1, pp. 64–76, Jul. 1998.

[15] S. Saxena, R. Sharma, and B. D. Pant, "Design and development of guided four beam cantilever type MEMS based piezoelectric energy harvester," *Microsyst. Technol.*, vol. 23, no. 6, pp. 1751–1759, Apr. 2016.

[16] C. Li, X. Y. Gao, T. T. Gao, J. Xiao, S. C. Fan, and W. Jin, "Analyzing the applicability of miniature ultra-high sensitivity Fabry–Pérot acoustic sensor using a nanothick graphene diaphragm," *Meas. Sci. Technol.*, vol. 26, no. 8, Jul. 2015, Art. no. 085101.

[17] C. Ma, B. Dong, J. M. Gong, and A. B. Wang, "Decoding the spectra of low-finesse extrinsic optical fiber Fabry–Pérot interferometers," *Opt. Express*, vol. 19, no. 24, pp. 23727–23742. Nov. 2011.

[18] *SPECIFICATIONS: Ultra Narrow Linewidth Laser Box, DL-BF9-CLSB-S, Rev. A*, DenseLight Semiconductors, Singapore, 2009, pp. 1–6.

[19] J. Ma, H. Xuan, H. L. Ho, W. Jin, Y. Yang, and S. Fan, "Fiber-optic Fabry–Pérot acoustic sensor with multilayer graphene diaphragm," *IEEE Photon. Technol. Lett.*, vol. 25, no. 10, pp. 932–935, May 2013.

[20] *USER GUIDE: Extended InGaAs Biased Detector, DET10N2, Rev. A*, Thorlabs, Newton, NJ, USA, 2017, pp. 1–17.

[21] *PRODUCT DATA: Free-field Microphone-Type 4190, DET10N2, Rev. A*, Brüel & Kjær, Nærum, Denmark, 2009, pp. 1–2.

[22] W. Jo, O. Kilic, and M. J. F. Digonnet, "Highly sensitive phase-front-modulation fiber acoustic sensor," *J. Lightw. Technol.*, vol. 33, no. 20, pp. 4377–4383, Oct. 15, 2015.

[23] W. Jo, O. C. Akkaya, O. Solgaard, and M. J. F. Digonnet, "Miniature fiber acoustic sensors using a photonic-crystal membrane," *Opt. Fiber Technol.*, vol. 19, no. 6, pp. 785–792, Dec. 2013.

XIAOGUANG QI was born in Shandong, China, in 1987. He received the B.S. degree from Qingdao Agricultural University, Qingdao, in 2010, and the M.Eng. degree from Tianjin Polytechnic University, Tianjin, China, in 2013. He is currently pursuing the Ph.D. degree in optoelectronics and photonics technology with Tianjin University, Tianjin, under the supervision of Prof. T. Liu.

His research interest includes on F-P fiber sensing.

SHUANG WANG was born in Tianjin, China, in 1982. She received the B.S. degree from Shandong University, China, in 2005, and the M.S. degree from Tianjin University, Tianjin, in 2007.

She is currently an Associate Professor at Tianjin University. Her research interests include optical fiber sensing and demodulation algorithm.

JUNFENG JIANG received the B.S. degree from the Southwest Institute of Technology, China, in 1998, and the M.S. and Ph.D. degrees from Tianjin University, Tianjin, China, in 2001 and 2004, respectively.

He is currently a Professor at Tianjin University. His research interests include fiber sensors and optical communication performance measurement.

KUN LIU received the B.Eng., M.Eng., and Ph.D. degrees from Tianjin University, Tianjin, China, in 2004, 2006, and 2009, respectively.

He is currently a Professor at Tianjin University. His research interests include fiber physics and chemistry sensing systems.

PENG ZHANG was born in Shanxi, China, in 1994. He received the B.S. degree from the University of Electronic Science and Technology of China, Chengdu, China, in 2013. He is currently pursuing the Ph.D. degree in optical engineering with Tianjin University, Tianjin, China, under the supervision of Prof. J. Jiang.

His research interest includes optical fiber F-P acoustic sensing.

ZHIYUAN LI was born in Henan, China, in 1996. He received the B.S. degree from Central South University, Changsha, in 2015. He is currently pursuing the Ph.D. degree in optoelectronics and photonics technology with Tianjin University, Tianjin, China, under the supervision of Prof. T. Liu.

His research interest includes F-P fiber sensing.

TIEGEN LIU received the B.Eng., M.Eng., and Ph.D. degrees from Tianjin University, Tianjin, China, in 1982, 1987, and 1999, respectively.

He is currently a Professor at Tianjin University. He is also a Chief Scientist of the National Basic Research Program of China under Grant 2010CB327802. His research interests include photoelectric detection and fiber sensing.